NANO LETTERS

pubs.acs.org/NanoLett Letter

Atomic-Scale Rectification and Inelastic Electron Tunneling Spectromicroscopy

Jiang Yao, Peter J. Wagner, Yunpeng Xia, Gregory Czap, and W. Ho*

Cite This: https://doi.org/10.1021/acs.nanolett.2c02503 Read Online

ACCESS | Metrics & More | Article Recommendations | Supporting Information

ABSTRACT: The phenomenon of rectification describes the emergence of a DC current from the application of an oscillating voltage. Although the origin of this effect has been associated with the nonlinearity in the current−voltage $I(V)$ relation, a rigorous understanding of the microscopic mechanisms for this phenomenon remains challenging. Here, we show the close connection between rectification and inelastic electron tunneling spectroscopy and microscopy for single molecules with a scanning tunneling microscope. While both techniques are based on nonlinear features in the $I(V)$ curve, comprehensive line shape analyses reveal notable differences that highlight the two complementary techniques of nonlinear conductivity spectromicroscopy for probing nanoscale systems.

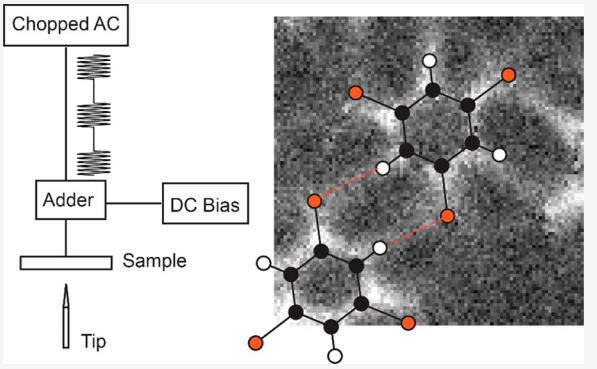

KEYWORDS: *rectification, inelastic electron tunneling, molecular vibrations, submolecular contrast, inelastic tunneling probe, scanning tunneling microscope*

Rectification spectroscopy probes system excitations by measuring the DC response to an AC perturbation of bulk materials[1−5] to nanoscale devices.[6−8] When it is measured with a scanning tunneling microscope (STM), rectification spectroscopy can characterize the spin[9] and vibration[10] excitation of single molecules. Moreover, resonant rectification spectromicroscopy (ESR-STM and THz-STM) simultaneously provides μeV energy resolution and atomic-scale spatial resolution.[11−17] Calibration of the RF amplitude in ESR-STM was obtained from the dependence of the rectification current on the RF field.[11,13−16] Results from THz-STM measurements often mixed effects of the THz field and the dynamical signal of the molecule.[17] Therefore, it has become a consequential analysis of rectification spectromicroscopy, in order to effectively use it for probing the static and dynamic properties of molecules and nanoscale systems.

Both the rectification (R) and inelastic electron tunneling spectroscopy (IETS) probe the $I(V)$ nonlinearity of a tunneling junction by measuring the DC and second harmonic (2ω) response in current to an AC bias modulation, $V_m \cos(\omega t)$, as a function of the DC bias V_B.[9,10,18−20] Based on the Taylor expansion to the second order, the line shapes of these two types of spectra should be identical with characteristic $\frac{d^2I}{dV^2}$ dependence:[9,10,19,20]

$$I_{2\omega}(V_B, V_m) = I_R(V_B, V_m) = \frac{1}{4}{V_m}^2 \frac{d^2I}{dV^2}\bigg|_{V_B} + (\text{higher-order terms in } V_m) \quad (1)$$

However, the consequences of such an approximation need to be assessed. While Paul et al. estimated with an oversimplified model the rectification signal strength at the molecular excitation energy,[11] a comprehensive line shape study of R-spectra is still missing.

Here, we examine the rigor of $\frac{d^2I}{dV^2}$ spectral analysis by comparing the line shapes for R and 2ω spectroscopy and how the line shapes affect the image contrast in spectromicroscopy. The experimental setups for measuring the R- and 2ω-spectra are shown in Figure 1. The R- and 2ω-spectra can yield similar results in measuring the inelastic electron tunneling (IET) induced nonlinearity,[10] as confirmed by the vibrational excitations of a single CO molecule (Figure 2a) in an STM junction (Figure 2b,c). The low (~2 meV) and high (~19 meV) energy peaks indicate the hindered translation (HT) and

Received: June 25, 2022
Revised: September 19, 2022

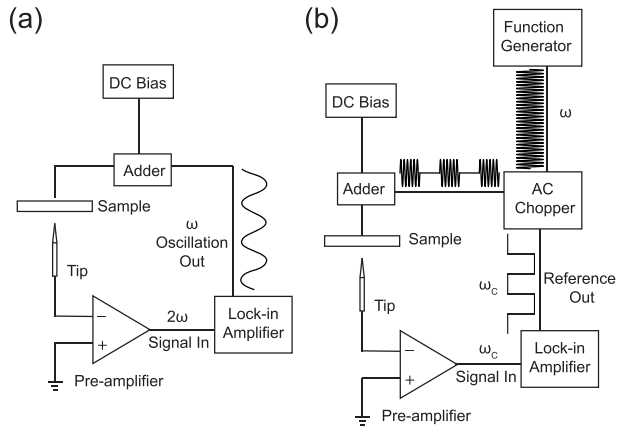

Figure 1. Experimental setups of two spectral techniques. (a) Second harmonic (2ω) inelastic electron tunneling spectroscopy (IETS). An AC bias modulation with a frequency of ω was fed into the tunneling junction. The lock-in amplifier measures the tunneling current oscillating at the 2ω frequency. (b) Rectification (R) spectroscopy. The bias modulation of frequency ω was generated by a function generator and square-wave chopped with a frequency of ω_C. The chopped bias modulation was fed into the tunneling junction. The lock-in amplifier measures the rectification current at the ω_C frequency.

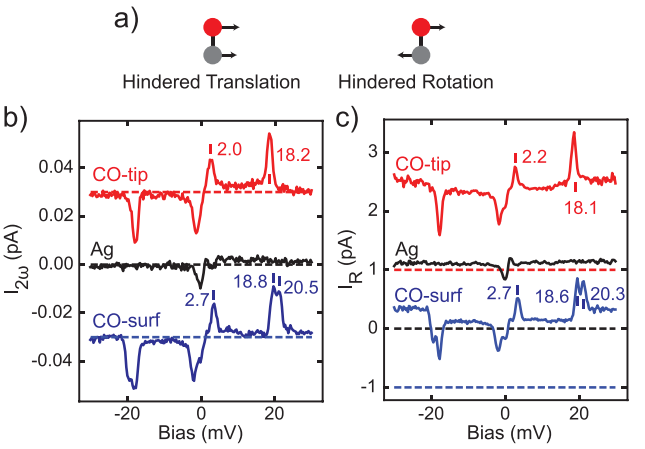

Figure 2. Two methods of single-molecule spectroscopy. (a) Schematic diagrams showing the hindered translation (HT) and hindered rotation (HR) vibrational modes of CO. (b) 2ω-spectra and (c) R-spectra measured with a Ag tip over a CO molecule adsorbed on an atop site of Ag(110) (blue), Ag tip over Ag(110) (black), and CO tip over Ag(110) (red). The experimental methods are described elsewhere for the R-spectra[9,10,17] and 2ω-spectra.[24,26,27] For all spectra, the feedback set point was 10 mV/300 pA, and the sample bias oscillation was 1 mV_{RMS} at 1 kHz. The square-wave chopping frequency used in the R-spectra was 471 Hz. The blue and red curves in panels b and c are offset for clarity with zero signal level indicated by the dashed lines. The offset and nonflat baseline in the R-spectra could result from the instrumental effects of the operational amplifier-based adder and returning loop through shared electrical power lines (see the Supporting Information). The zero offset was observed to be much smaller using the discrete inductor and capacitor-based bias tee for the adder in Figure 1.

rotation (HR) modes of CO (Figure 2a).[21−23] Doublet splitting affects the line shape of HR and HT peaks for CO adsorbed on the anisotropic Ag(110) surface.[21,23] Additionally, the low HT energy and the thermal and modulation spectral

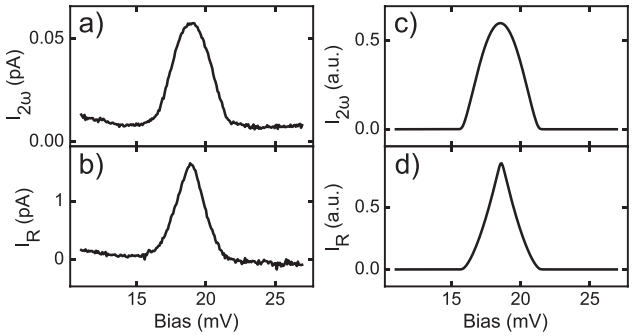

Figure 3. Comparison of 2ω and R spectral line shapes. (a) Experimental and (c) simulated spectra of the HR peak on the positive bias side for the CO tip over Ag(110), acquired by the IETS 2ω spectroscopy. (b) Experimental and (d) simulated spectra of the same CO tip over Ag(110) measured by the R spectroscopy with 471 Hz square-wave chopping frequency. For all spectra, the feedback set point was 10 mV/300 pA, and the sample bias sinusoidal oscillation was 2 mV_{RMS} at 1 kHz. The excitation energy for the simulated spectra was chosen to be the same as the corresponding experimental peak position. The temperature and oscillation RMS amplitude used in the calculated spectra were the same as those in the experiment: 0.6 K and 2 mV_{RMS}.

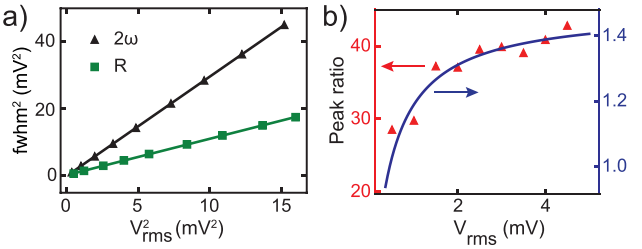

Figure 4. Comparison of line width and intensity of 2ω- and R-spectra. (a) Squared full width at half-maximum (fwhm) of 2ω-spectra (black triangles) and R-spectra (green squares), as a function of the squared RMS oscillation amplitude. The measured spectra were fitted by a simulated line shape with the fwhm and peak height derived from fitting parameters. The lines are the best linear fit of the experimental data. The slopes for the black (2ω) and green (R) lines are 2.96 and 1.08 with corresponding y-intercepts of 0.012 and 0.250. (b) Simulated (blue curve) and experimental (red triangle) peak ratio, $H_R/H_{2\omega}$, from the 2ω- and R-spectra, versus the RMS amplitude of the bias oscillation.

Table 1. Summary of Key Features Calculated for the Rectification and Second Harmonic Signals[a]

R = rectification; 2ω = second harmonic	peak height	fwhm	integrated area	peak−width ratio
sinusoidal wave R	V_m/π	$0.72V_m$	$V_m^2/4$	0.442
square wave R	$V_m/2$	V_m	$V_m^2/2$	0.500
triangle wave R	$V_m/4$	$0.59V_m$	$V_m^2/6$	0.427
sinusoidal wave 2ω	$2V_m/(3\pi)$	$1.22V_m$	$V_m^2/4$	0.174

[a]Rectification spectra were calculated for three different voltage oscillations: sinusoidal wave, square wave, and triangular wave. The analytical forms of the instrumental function are given in the Supporting Information. The second harmonic spectrum was calculated for sinusoidal voltage oscillation.

broadening lead to interference of the HT features on the positive and negative biases. Therefore, we selected the HR

https://doi.org/10.1021/acs.nanolett.2c02503
Nano Lett. XXXX, XXX, XXX−XXX

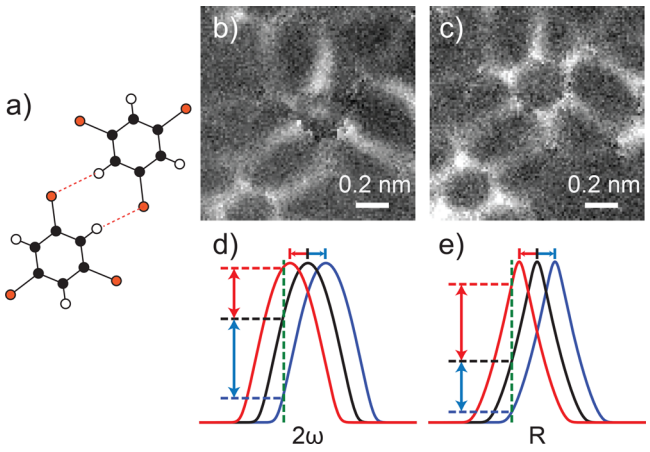

Figure 5. R vs 2ω spectromicroscopy. (a) Schematic diagram showing the interactions (dashed red lines) between two 2,4,6-tribromobenzene molecules. (b) itProbe image of the 2ω signal, showing the intermolecular interactions between two 2,4,6-tribromobenzene molecules acquired at 1.5 mV sample bias (red-shifted HT mode) and 1 mV_{RMS} sine-wave bias oscillation at 471 Hz. (b) rProbe image of the R signal acquired with the same CO tip, scanned area, and conditions except with 1 kHz bias oscillation and 471 Hz square-wave chopping frequency. Images in panels b and c were acquired at constant height with the feedback turned off at 100 mV/100 pA over the middle of the molecule nearest to the center of the image and advancing the tip 1.68 Å toward the surface prior to measuring the signals. Molecules were evaporated and self-assembled on Ag(110) at 25 K, and imaged at 600 mK. (d, e) Illustration of the contrast differences between itProbe and rProbe induced by the corresponding spectral line shapes. The black, red, and blue lines are the unperturbed, red-shifted, and blue-shifted HT peak of the CO tip. The vertical green lines indicate the bias position relative to the unperturbed peak used in the spectromicroscopy. The double-sided red and blue arrows are the signal variations induced by the corresponding shifts; higher contrast is obtained for a larger difference in the lengths of the arrows for each Probe.

peak of CO adsorbed on the tip (CO tip) over Ag(110) for the line shape analyses between these two types of spectroscopy. This feature is doubly degenerated and isolated because of the symmetric binding configuration for the CO tip.[23]

The 2ω-spectrum for the CO tip over Ag(110) substrate yields a bell-shaped HR peak, while the corresponding R-spectrum exhibits a peak of triangular shape (Figure 3a,b). The simulated 2ω-spectrum based on its theoretical form, $\frac{d^2I}{dV_B^2} * \phi_{2\omega}(V_B)$,[24−26] agrees with the experimental data (Figure 3a,c). The $*$ stands for the convolution of two functions, and $\phi_{2\omega}(V_B)$ is the 2ω instrumental function (shown as eq S38 in the Supporting Information).[25] However, the response function for the R-spectrum has previously not been derived and is given below (see the Supporting Information for details of its derivation):

$$I_R(V_B) = \frac{d^2I}{dV_B^2} * \phi_R(V_B) \tag{2}$$

$\Phi_R(V_B)$ is the instrumental function for the rectification method, which depends on the waveform of bias modulation used. Each AC modulation waveform has a unique voltage probability distribution, $D(V_B)$, which relates to $\Phi_R(V_B)$ with the following relation (see the Supporting Information for details of its derivation):

$$\phi_R(V_B) = \int (D(V_B) - \delta(V_B))\, dV_B \tag{3}$$

For a sinusoidal voltage oscillation, the instrumental function, $\Phi_R(V_B)$, takes the following form:

$$\phi_R(V_B) = \begin{cases} \dfrac{\arcsin\left(\frac{|V_B|}{V_m}\right)|V_B|}{\pi} - \dfrac{|V_B|}{2} + \dfrac{\sqrt{V_m^2 - V_B^2}}{\pi} & \text{if } |V_B| < V_m \\ 0 & \text{if } |V_B| \geq V_m \end{cases} \tag{4}$$

The simulated R-spectrum line shape agrees with the measured triangular shape (Figure 3b,d). At low temperatures, $\frac{d^2I}{dV_B^2}$ of IET resembles delta functions centered at molecular excitation energies,[24,25] and eq 2 approximates $\Phi_R(V_B)$, which yields a peak height of $\frac{V_m}{\pi}$ and a full width at half-maximum (fwhm) of $0.72V_m$.

The different spectral line shapes of IETS and rectification peaks deviate from the $\frac{d^2I}{dV^2}$ interpretation. To understand this deviation, we inspected the origin of $\frac{d^2I}{dV^2}$ interpretation involving the Taylor expansion of the $I(V)$ function. Performing the Taylor expansion of any function requires the convergence of its corresponding series. However, we calculated the Taylor series of IET $I(V)$ with different V_m and found that the series converged conditionally; V_m needed to be smaller than a certain value to make it converge (see Figure S4 in the Supporting Information). For the bias amplitude used in this report ($V_m \geq 0.5$ mV), the Taylor series of IET $I(V)$ always diverges, which nullifies the $\frac{d^2I}{dV^2}$ interpretation. We observed that the Taylor series started to converge with V_m = 0.1 mV, where the $\frac{d^2I}{dV^2}$ served as a good approximation for both R- and 2ω-spectra. However, with such a small bias modulation, the IET signal can be too weak to detect. Nonetheless, the 2ω- and R-spectra still correlate with $\frac{d^2I}{dV^2}$, and their peak positions indicate the excitation energies (see the Supporting Information). However, when multiple peaks are close to each other, the correct mathematical form for the line shape must be applied to accurately determine the excitation energies.

For IETS, the line width and height of excitation peaks represent the energy resolution and signal strength.[26] The R- and 2ω-spectra have similar convolutional form,[27] and their fwhm's follow eq 5:

$$\text{fwhm}^2 = W_{\text{intrinsic}}^2 + KV_{\text{rms}}^2 + \left(\frac{5.4k_BT}{e}\right)^2 \tag{5}$$

where k_B and T are the Boltzmann constant and temperature. The intrinsic broadening, $W_{\text{intrinsic}}$, of CO molecules is negligible. KV_{rms}^2 is the square of the corresponding instrumental function fwhm, and the theoretical K values are 2.97 for the 2ω-spectra and 1.04 for the R-spectra (see the Supporting Information). We observed the linear relationship between fwhm^2 and V_{rms}^2 with fitted slopes of 2.96 (2ω-spectra) and 1.08 (R-spectra), which agrees with the theoretical K values (Figure 4a). In addition, for V_{rms} values

https://doi.org/10.1021/acs.nanolett.2c02503
Nano Lett. XXXX, XXX, XXX−XXX

used in Figure 4a, R-spectra have smaller line widths compared with 2ω-spectra and thus yield higher energy resolution.

To compare the signal strength of these two types of spectra, we studied their peak height ratio, $H_R/H_{2\omega}$, as a function of V_{rms}. The trend of measured $H_R/H_{2\omega}$ resembles the calculated curve, but the absolute values are higher than the calculated results by over an order of magnitude (Figure 4b). The reasons for such a difference are as follows: In 2ω and R measurements, the preamplifier extracts the 2 kHz (twice the bias modulation frequency) and 471 Hz (ω_C, chopping frequency) component in the tunneling current, respectively (Figure 1). The amplification of the preamplifier decreases as the frequency increases for the detected signal for the tunneling current. Therefore, the measurement yielded an H_R 20−40 times larger than $H_{2\omega}$, while theory predicts an $H_R/H_{2\omega}$ slightly larger than 1. If the bias modulation frequency of the 2ω-spectra is half of the R-spectra chopping frequency ($\omega = \omega_C/2$), the preamplifier extracts both spectra at the same frequency, and the measured $H_R/H_{2\omega}$ will closely follow the theoretical value. Under this condition, the noise level (which is also frequency dependent) will also be the same for 2ω- and R-spectra, which leads to the signal-to-noise ratio, $SNR_R/SNR_{2\omega}$, to be the same as $H_R/H_{2\omega}$. In addition, the calculated $H_R/H_{2\omega}$ values are greater than one unless using very small V_{rms} (Figure 4b). This suggests that R-spectra surpass 2ω-spectra in signal strength. Overall, the R-spectra exhibit higher energy resolution and signal strength compared to IETS 2ω-spectra.

Different bias modulation waveforms resulted in different rectification instrumental functions which could lead to better signal strength or smaller peak widths. In addition, the instrumental functions served as good approximations for large amplitude voltage oscillations. Therefore, we explored the $\Phi_R(V_B)$ of different bias modulation waveforms and summarized the key features in Table 1. All waveforms for the rectification method have a larger peak-to-width ratio, $H_{R(2\omega)}$/fwhm, than 2ω-spectra. The square wave rectification has the best peak-to-width figure of merit and the largest integrated area under the peak. Usually, there is a trade-off between signal strength and energy resolution. However, by manipulating the bias modulation waveform, the signal strength and energy resolution can be simultaneously improved. The THz-STM would also benefit by studying the waveforms for rectification spectroscopy. To our knowledge, all THz-STM to date used pulsed THz irradiation having nonstandard waveforms. However, if the waveforms can be properly calibrated, the corresponding $D(V_B)$ can be obtained. With eqs 2 and 3, the instrumental function and rectification signal can be derived. Such signals would be purely from the field effect of THz irradiation and usually mixed with the molecular dynamic response.[17] These two effects can be separated using our theoretical work presented here.

The line shape difference between R-spectra and 2ω-spectra also affects the corresponding spectromicroscopy contrast. The variation in surface potential shifts the HT peak of a CO tip and results in the 2ω signal variation at a certain bias.[22,28−30] Inelastic tunneling probe (itProbe) maps this 2ω signal variation and reveals molecular skeletal structures and intermolecular interactions.[28−30] The interactions and chemical bonds as depicted in Figure 5a are seen as the bright lines in the itProbe image of a 2,4,6-tribromobenzene cluster (Figure 5b). Following the same principle, rectification probe (rProbe) maps the corresponding R signal variations and achieves the same purpose (Figure 5c). However, we observed the contrast quality of the rProbe image to be better than that of itProbe (Figure 5b vs Figure 5c). We attribute this contrast improvement to the triangular peak shape of R-spectra. With the same amount of peak shift, the rProbe produces more signal variation than the itProbe for red shifts, but less for blue shifts (Figure 5d,e). The red shifts happen when the CO tip is positioned over the chemical bonding region, molecular interaction region, and nucleus positions; thus, rProbe provides enhanced contrast for these molecular features.

In summary, we demonstrated that R-spectra differ from 2ω-spectra, suggesting that the conventional $\frac{d^2I}{dV^2}$ understanding based on Taylor expansion is incomplete for these two types of spectromicroscopy based on the nonlinear $I(V)$ relation. Theoretical and experimental analyses of the line shapes for the R- and 2ω-spectra of a single CO molecule attached to the STM tip revealed that R-spectra surpass 2ω-spectra in the energy resolution and signal strength. Additionally, spectromicroscopy by rProbe leads to a superior contrast in images of the molecular structure and bonding compared to the itProbe. These advantages should lead to analyses of static and dynamic properties of nanoscale systems by rectification spectroscopy and microscopy.[17] Here, we provide the fundamental understanding and scientific basis of the atomic-scale rectification phenomena and spectromicroscopy based on measuring the rectification current.

■ ASSOCIATED CONTENT

Supporting Information

The Supporting Information is available free of charge at https://pubs.acs.org/doi/10.1021/acs.nanolett.2c02503.

Materials and Method section; Taylor expansion treatment; nonlinear tunneling current; instrumental function; maximum rectification signal; first harmonic signal; spectral fitting; and conditional convergence of Taylor expansion (PDF)

■ AUTHOR INFORMATION

Corresponding Author

W. Ho − *Department of Physics and Astronomy, University of California, Irvine, California 92697-4575, United States; Department of Chemistry, University of California, Irvine, California 92697-2025, United States;* orcid.org/0000-0003-3884-2142; Email: wilsonho@uci.edu

Authors

Jiang Yao − *Department of Physics and Astronomy, University of California, Irvine, California 92697-4575, United States;* orcid.org/0000-0001-5848-8000

Peter J. Wagner − *Department of Physics and Astronomy, University of California, Irvine, California 92697-4575, United States;* orcid.org/0000-0003-3138-6834

Yunpeng Xia − *Department of Physics and Astronomy, University of California, Irvine, California 92697-4575, United States;* orcid.org/0000-0001-5750-809X

Gregory Czap − *Department of Physics and Astronomy, University of California, Irvine, California 92697-4575, United States;* orcid.org/0000-0002-3209-3198

Complete contact information is available at: https://pubs.acs.org/10.1021/acs.nanolett.2c02503

https://doi.org/10.1021/acs.nanolett.2c02503
Nano Lett. XXXX, XXX, XXX−XXX

Notes

The authors declare no competing financial interest.

■ ACKNOWLEDGMENTS

This project was supported by the Office of Naval Research under Grant N00014-20-1-2475. We have additionally benefitted from discussions with and suggestions by Siyu Chen, Likun Wang, Wenlu Shi, and Dan Bai.

■ REFERENCES

(1) D'Amico, G.; Pesce, G.; Rusciano, G.; Sasso, A. A DFG spectrometer at 3μm for high resolution molecular spectroscopy and trace gas detection. *Opt. Lasers Eng.* **2002**, *37* (5), 481−493.
(2) Bozzini, B.; Busson, B.; De Gaudenzi, G. P.; Mele, C.; Tadjeddine, A. An SFG and DFG investigation of polycrystalline Au, Au-Cu and Au-Ag-Cu electrodes in contact with aqueous solutions containing KCN. *J. Alloys Compd.* **2007**, *427* (1-2), 341−349.
(3) Bozzini, B.; Busson, B.; De Gaudenzi, G. P.; Mele, C.; Tadjeddine, A. An SFG and DFG investigation of Au(111), Au(100), Au(110) and Au(210) electrodes in contact with aqueous solutions containing KCN. *J. Solid State Electrochem.* **2008**, *12* (3), 303−313.
(4) Bozzini, B.; Bund, A.; Busson, B.; Humbert, C.; Ispas, A.; Mele, C.; Tadjeddine, A. An SFG/DFG investigation of CN- adsorption at an Au electrode in 1-butyl-1-methyl-pyrrolidinium bis-(trifluoromethylsulfonyl) amide ionic liquid. *Electrochem. commun.* **2010**, *12* (1), 56−60.
(5) Vogelsang, J.; Robin, J.; Piglosiewicz, B.; Manzoni, C.; Farinello, P.; Melzer, S.; Feru, P.; Cerullo, G.; Lienau, C.; Groß, P. High passive CEP stability from a few-cycle, tunable NOPA-DFG system for observation of CEP-effects in photoemission. *Opt. Express* **2014**, *22* (21), 25295−25306.
(6) Sankey, J. C.; Braganca, P. M.; Garcia, A. G. F.; Krivorotov, I. N.; Buhrman, R. A.; Ralph, D. C. Spin-transfer-driven ferromagnetic resonance of individual nanomagnets. *Phys. Rev. Lett.* **2006**, *96* (22), 227601.
(7) Cheng, X.; Boone, C. T.; Zhu, J.; Krivorotov, I. N. Nonadiabatic Stochastic Resonance of a Nanomagnet Excited by Spin Torque. *Phys. Rev. Lett.* **2010**, *105* (4), 47202.
(8) Cheng, X.; Katine, J. A.; Rowlands, G. E.; Krivorotov, I. N. Nonlinear ferromagnetic resonance induced by spin torque in nanoscale magnetic tunnel junctions. *Appl. Phys. Lett.* **2013**, *103* (8), 82402.
(9) Lee, J.; Tu, X.; Ho, W. Spectroscopy and Microscopy of Spin-Sensitive Rectification Current Induced by Microwave Radiation. *Nano Lett.* **2005**, *5* (12), 2613−2617.
(10) Tu, X. W.; Lee, J. H.; Ho, W. Atomic-scale rectification at microwave frequency. *J. Chem. Phys.* **2006**, *124* (2), 21105.
(11) Paul, W.; Baumann, S.; Lutz, C. P.; Heinrich, A. J. Generation of constant-amplitude radio-frequency sweeps at a tunnel junction for spin resonance STM. *Rev. Sci. Instrum.* **2016**, *87* (7), 74703.
(12) Cocker, T. L.; Peller, D.; Yu, P.; Repp, J.; Huber, R. Tracking the ultrafast motion of a single molecule by femtosecond orbital imaging. *Nature* **2016**, *539* (7628), 263−267.
(13) Choi, T.; Lutz, C. P.; Heinrich, A. J. Studies of magnetic dipolar interaction between individual atoms using ESR-STM. *Curr. Appl. Phys.* **2017**, *17* (11), 1513−1517.
(14) Willke, P.; Paul, W.; Natterer, F. D.; Yang, K.; Bae, Y.; Choi, T.; Fernández-Rossier, J.; Heinrich, A. J.; Lutz, C. P. Probing quantum coherence in single-atom electron spin resonance. *Sci. Adv.* **2018**, *4* (2), No. eaaq1543.
(15) Willke, P.; Singha, A.; Zhang, X.; Esat, T.; Lutz, C. P.; Heinrich, A. J.; Choi, T. Tuning single-atom electron spin resonance in a vector magnetic field. *Nano Lett.* **2019**, *19* (11), 8201−8206.
(16) Yang, K.; Paul, W.; Phark, S.-H.; Willke, P.; Bae, Y.; Choi, T.; Esat, T.; Ardavan, A.; Heinrich, A. J.; Lutz, C. P. Coherent spin manipulation of individual atoms on a surface. *Science* **2019**, *366* (6464), 509−512.
(17) Wang, L.; Xia, Y.; Ho, W. Atomic-scale quantum sensing based on the ultrafast coherence of an H2 molecule in an STM cavity. *Science* **2022**, *376* (6591), 401−405.
(18) Völcker, M.; Krieger, W.; Walther, H. A Laser-Driven Scanning Tunneling Microscope. *AIP Conf. Proc.* **1991**, *241* (1), 51−60.
(19) Bragas, A. V.; Landi, S. M.; Martınez, O. E. Laser field enhancement at the scanning tunneling microscope junction measured by optical rectification. *Appl. Phys. Lett.* **1998**, *72* (17), 2075−2077.
(20) Ward, D. R.; Hüser, F.; Pauly, F.; Cuevas, J. C.; Natelson, D. Optical rectification and field enhancement in a plasmonic nanogap. *Nat. Nanotechnol.* **2010**, *5* (10), 732−736.
(21) Xu, C.; Chiang, C.; Han, Z.; Ho, W. Nature of asymmetry in the vibrational line shape of single-molecule inelastic electron tunneling spectroscopy with the STM. *Phys. Rev. Lett.* **2016**, *116* (16), 166101.
(22) Han, Z.; Czap, G.; Xu, C.; Chiang, C.; Yuan, D.; Wu, R.; Ho, W. Probing intermolecular coupled vibrations between two molecules. *Phys. Rev. Lett.* **2017**, *118* (3), 36801.
(23) Czap, G.; Han, Z.; Wagner, P. J.; Ho, W. Detection and Characterization of Anharmonic Overtone Vibrations of Single Molecules on a Metal Surface. *Phys. Rev. Lett.* **2019**, *122* (10), 106801.
(24) Lambe, J.; Jaklevic, R. C. Molecular vibration spectra by inelastic electron tunneling. *Phys. Rev.* **1968**, *165* (3), 821.
(25) Klein, J.; Léger, A.; Belin, M.; Défourneau, D.; Sangster, M. J. L. Inelastic-electron-tunneling spectroscopy of metal-insulator-metal junctions. *Phys. Rev. B* **1973**, *7* (6), 2336.
(26) Stipe, B. C.; Rezaei, M. A.; Ho, W. Single-Molecule Vibrational Spectroscopy and Microscopy. *Science* **1998**, *280* (5370), 1732−1735.
(27) Lauhon, L. J.; Ho, W. Effects of temperature and other experimental variables on single molecule vibrational spectroscopy with the scanning tunneling microscope. *Rev. Sci. Instrum.* **2001**, *72* (1), 216−223.
(28) Chiang, C.; Xu, C.; Han, Z.; Ho, W. Real-space imaging of molecular structure and chemical bonding by single-molecule inelastic tunneling probe. *Science* **2014**, *344* (6186), 885−888.
(29) Han, Z.; Wei, X.; Xu, C.; Chiang, C.; Zhang, Y.; Wu, R.; Ho, W. Imaging van der Waals interactions. *J. Phys. Chem. Lett.* **2016**, *7* (24), 5205−5211.
(30) Han, Z.; Czap, G.; Chiang, C.; Xu, C.; Wagner, P. J.; Wei, X.; Zhang, Y.; Wu, R.; Ho, W. Imaging the halogen bond in self-assembled halogenbenzenes on silver. *Science* **2017**, *358* (6360), 206−210.

https://doi.org/10.1021/acs.nanolett.2c02503
Nano Lett. XXXX, XXX, XXX−XXX